Journal of Electrical Engineering, Vol. 77, No. 1, 2026, pp. 21-32
https://reference-global.com/journal/JEE

BPG bits per pixel prediction via linear mapping from JPEG compression

Boban P. Bondžulić[1], Vladimir V. Lukin[2], Nenad M. Stojanović[1], Andrii S. Adamovych[2]

This paper addresses the challenge of predicting the compression performance of the computationally complex Better Portable Graphics (BPG) image codec without executing its demanding encoding process. We propose a novel methodology that leverages a linear mapping between the bits per pixel (bpp) of JPEG and BPG compressed images. The core of the approach involves determining optimal pairs of JPEG Quality Factor (QF) and BPG quantization parameter (Q) that maximize bpp correlation, and deriving corresponding linear mapping laws. These laws, established once on a training set, enable BPG bpp prediction for any new image using only a fast JPEG compression. The method was rigorously validated on a diverse dataset including color, grayscale, and infrared images from both the same and different sensor systems. Results demonstrate high prediction accuracy with a Mean Relative Error (MRE) below 8.6% within the training sensor domain and robust generalization to external sensors, where the MRE remains below 11.2% across all image types. This work provides a practical and efficient solution for bpp prediction in scenarios where computational resources or time are constrained, facilitating informed compression decisions prior to committing to intensive BPG encoding.

Keywords: image compression, BPG, JPEG, bits per pixel prediction, linear mapping, cross-codec prediction, computational efficiency, generalization

1 Introduction

Image compression is a fundamental tool for efficient data storage and transmission, given the ever-increasing volume of visual data [1]. Compression techniques are broadly categorized into lossless, lossy, and visually lossless methods [1, 2]. While lossless compression preserves all original information, it offers limited compression ratio (CR). For many applications, lossy compression is indispensable to achieve significantly smaller file sizes, accepting a controlled loss of information. The performance of any compression technique is evaluated based on three key, and often conflicting criteria: the quality of the output signal, the compression ratio (often expressed as file size or bits per pixel – bpp), and computational complexity [2, 3].

The compression process is typically controlled by a parameter that controls compression (PCC), which is specific to the encoder's implementation. Common examples include the Quality Factor (QF) used in JPEG and WebP encoders, the Quantization Parameter (QP) found in video and image codecs like High-Efficiency Video Coding (HEVC) and Versatile Video Coding (VVC), Quantization Step (QS) found in AGU encoder, the parameter Q specific to the Better Portable Graphics (BPG) encoder, and a target compression ratio, which can be set in wavelet-based coders such as JPEG2000 and SPIHT. These allow a user to indirectly trade off quality for file size. However, the relationship between a specific PCC value and the resulting quality or bpp is highly dependent on the input image's characteristics, making precise control challenging [4]. While some researchers have proposed using custom, image-adaptive quantization tables instead of conventional empirically designed ones to improve this trade-off [5, 6], a common brute-force solution is iterative encoding-decoding. This process adjusts the PCC iteratively until a target quality or file size is met within acceptable tolerances, but it is computationally very expensive and impractical for real-time applications [7, 8].

Furthermore, it is crucial to consider the computational efficiency of the encoding and decoding process, which varies significantly across different codecs [9]. While modern codecs like BPG and the upcoming VVC standard offer superior compression efficiency compared to older standards like JPEG, this improvement is primarily achieved by making the encoding and decoding algorithms substantially more complex. As a result, these state-of-the-art codecs are often far from achieving real-time performance, especially for the demanding task of generating high-quality compressed images [10]. This inherent trade-off underscores the importance of prediction models that can circumvent the need for iterative or brute-force encoding, saving significant time and resources.

[1] Military Academy, University of Defence in Belgrade, 11000 Belgrade, Serbia
[2] Department of Information-Communication Technologies, National Aerospace University, 61070 Kharkiv, Ukraine
bondzulici@yahoo.com, v.lukin@khai.edu, nivzvk@hotmail.com, andriy.adamovych@gmail.com

https://doi.org/10.2478/jee-2026-0003, Print (till 2015) ISSN 1335-3632, On-line ISSN 1339-309X

This challenge highlights the significant value of predicting compression performance prior to the actual coding process [11]. Accurate pre-compression prediction of metrics like bpp enables the selection of the most suitable compression algorithm, informed decision-making for PCC values, and efficient bit allocation in memory [6, 12-14]. Consequently, various approaches for predicting image quality, bpp and CR have been explored. These methods typically employ simple features extracted from the original image, such as mean gradient magnitude [15], image activity measure [12, 14], differential information entropy [16], local activity in blocks [17], or statistics from frequency-domain transforms like DCT [18-20], and have been applied to various codecs including JPEG, JPEG XR, WebP, BPG, SPIHT and JPEG2000 [20-24].

In this context, we propose a novel method for predicting the bpp of BPG compressed images without performing the actual BPG compression. The foundation of our work is the established linear relationship between the bpp values of JPEG and BPG compressed images at the first Just Noticeable Difference (JND#1) points, as demonstrated in our earlier research [25]. This paper calculates the correlation between bpp across the entire parameter value space for JPEG (quality factor QF from 1 to 100) and BPG (parameter Q from 0 to 51). Our goal is to predict the bpp of a BPG compressed image for one, multiple, or all values of Q. This is achieved by leveraging the bpp of a JPEG compressed image and a set of pre-determined linear mapping laws that translate JPEG bpp to BPG bpp for all 52 possible Q values.

The proposed approach is rigorously tested and validated on a comprehensive and representative image dataset. This dataset has been designed to evaluate the robustness and generality of the mapping laws and it includes color images, their grayscale conversions, and specific grayscale infrared images obtained using sensors operating in the invisible (infrared) part of the electromagnetic spectrum. The inclusion of this diverse imagery, particularly the infrared data which possesses distinct statistical properties, demonstrates the wide applicability of our method beyond conventional photographic content. By using these mapping laws, one can accurately predict the compression efficiency of the BPG codec for a given image, entirely bypassing the computationally intensive BPG encoding process. This approach is particularly valuable in scenarios requiring high-quality compression, where using complex codecs like BPG or VVC can take significantly longer than real time [10, 26, 27]. We expect to have accurate bpp (CR) prediction applicable to different types of images.

The remainder of this paper is structured as follows. Section 2 details the materials and methods describing the dataset, the compression framework, and the proposed prediction methodology based on linear mapping laws between JPEG and BPG bpp. Section 3 presents the experimental results and analysis beginning with the establishment of the optimal mapping laws and their illustration, followed by a comprehensive performance evaluation under both intra-dataset and cross-dataset scenarios for color, grayscale, and infrared images. Finally, Section 4 concludes the paper by summarizing the main findings and suggesting directions for future research.

2 Materials and methods

Our previous research confirmed that information about the boundary between the visually lossless and visually lossy domains (JND#1) for one compression type can be successfully leveraged to determine the corresponding threshold for another compression type [25]. This transfer of information demonstrated bidirectionality, explicitly confirmed in [25] for the relationship between JPEG and BPG color image compression, where a linear relationship between their bpp values at this threshold was also observed. As a logical continuation of these findings, the idea emerged to extend the analysis of the bpp relationship between JPEG and BPG compressions to the entire space of possible PCC values, moving beyond the exclusive focus on the specific JND threshold case. To train and rigorously test a model based on this idea, a representative dataset of images was used, encompassing captures from the visible spectrum (both color and grayscale) and the infrared spectrum.

2.1 Dataset description and experimental setup

During the phase that can be treated as a specific training, a set of 25 images from the M^3FD dataset [28] was utilized. This set comprised spatially aligned (registered) triplets consisting of original 24-bit color images, their 8-bit grayscale conversions, and corresponding 8-bit infrared images. The image content included common objects and scenes such as people, cars, buses, motorcycles, lamps, trucks, and buildings. The data was captured using a synchronized sensor system containing one binocular optical camera and one binocular infrared sensor, with grayscale versions subsequently derived from the color images.

The testing phase was conducted through two distinct scenarios to evaluate the model's robustness and generalizability. In the first scenario (Scenario 1), another set of 25 images (24-bit color, 8-bit grayscale, and 8-bit infrared) was selected from the same M^3FD database, captured by the same sensor system. These images were carefully chosen to match the content profile of the training set.

In the second, more challenging Scenario 2, a different set of 20 high-resolution color images was compiled from external sources to test cross-dataset performance. Ten images were sourced from the JPEG XR database [29], and ten were randomly selected from the 50 available images in the MCL-JCI database [30] (grayscale versions are derived from these color images). These source images are characterized by higher resolution, a wider color gamut, and excellent visual quality, though the specific sensor origins are unknown. Crucially, for this scenario, the infrared images do not correspond to the same scenes as the color/grayscale set. They were sourced from a publicly available infrared image database and were captured using four different sensor systems [31], introducing significant variability.

2.2 Compression framework

The core of this study revolves around a comparative analysis between the widely adopted JPEG standard and the modern BPG format. JPEG compression, based on the DCT, operates by converting 8×8 pixel blocks into the frequency domain, followed by quantization and entropy coding. The compression level is primarily controlled by quality factor, QF, which directly influences the quantization matrices; a lower QF results in more aggressive quantization, higher compression, and lower image fidelity. In contrast, BPG utilizes the intra-frame coding techniques of the HEVC standard, offering a more advanced compression framework [32, 33]. It employs larger block sizes and a more sophisticated set of prediction modes, leading to, in general, superior rate-distortion performance compared to JPEG. The BPG compression is governed by a quantization parameter (Q), where a higher Q value corresponds to a larger quantization step, resulting in a smaller file size and a higher degree of information loss. The fundamental difference in their underlying architectures is the key reason for BPG's efficiency advantage, albeit at the cost of significantly higher computational complexity during encoding and decoding. This research directly builds upon the foundation established in [25], which utilized the BPG chroma subsampling format 4:2:2. To ensure consistency, the 4:2:2 chroma format has been adopted in this work as well.

2.3 Proposed prediction methodology

The core of our method lies in establishing a direct mapping between the bpp of a JPEG compressed image and the bpp of a BPG compressed version of the same image. The proposed framework operates in two distinct phases: a one-time, off-line training (in advance) phase, and a subsequent prediction phase applicable to any image at hand.

2.3.1 Training (mapping) phase

This initial, one-time phase is performed on the dedicated training dataset. For the entire set of training images, we systematically compress each image using both the JPEG and BPG codecs across their full parameter spaces – specifically, JPEG with QF from 1 to 100 and BPG with parameter Q from 0 to 51. For each resulting compressed image, the bpp value is calculated. The core of this phase involves identifying, for each target BPG Q value, the optimal JPEG QF value that yields the strongest correlation between the bpp of the JPEG compressed images and the bpp of the BPG compressed images. These optimal (QF, Q) pairs are determined by selecting the pairing that maximizes the correlation coefficient for each Q. Subsequently, for each of these 52 optimal pairs (one for each BPG Q), a unique linear mapping law

$$bpp_{\mathrm{BPG}} = a \cdot bpp_{\mathrm{JPEG}} + b \tag{1}$$

is derived using linear regression. These mapping laws and the corresponding optimal parameter pairs are determined once and for all and are stored for use in the prediction phase.

2.3.2 Prediction phase

In this phase, the pre-established mapping laws are applied to a new, unseen test image to predict its BPG bpp without performing the actual BPG compression. The procedure is as follows: for a given test image and a desired target BPG Q value, the corresponding optimal JPEG QF is retrieved. The test image is then compressed into the JPEG format using this specific QF value. The bpp of this resulting JPEG file is calculated and used as the input to the corresponding pre-computed linear mapping law. By applying this law, the bpp of the BPG compressed image is accurately predicted.

2.4 Evaluation metrics

The accuracy of the proposed bpp prediction method has been quantitatively assessed using a comprehensive set of statistical metrics. The agreement between the predicted bpp values and the actual bpp values obtained from true BPG compression is measured through both correlation and error-based metrics.

To evaluate the strength and direction of the linear relationship, Pearson's correlation coefficient (LCC) is employed. Furthermore, to capture any monotonic (not necessarily linear) relationships, two rank correlation coefficients are calculated: Spearman's rank correlation coefficient (SRCC) and Kendall's rank correlation coefficient (KRCC). The magnitude of prediction errors was quantified using the Mean Absolute Error (MAE), the Root Mean Square Error (RMSE) – which is more sensitive to large errors, and the Mean Relative Error (MRE), which provides insight into the average relative deviation of the predictions.

To complement this global quantitative analysis and provide a more granular understanding of the model's performance, the results are also further analyzed through visual illustrations. The relationships between predicted and actual bpp are visualized across two key dimensions:

1. **By Q parameter sub-range:** The entire range of the BPG parameter Q is divided into five distinct sub-ranges to examine if prediction accuracy remains consistent across different compression intensities.
2. **Per image:** The performance is also visualized for each individual source image to identify any potential dependencies on specific image content or characteristics.

This multi-faceted evaluation strategy, combining global metrics with detailed visual analysis, ensures a robust and thorough validation of the prediction methodology's effectiveness.

3 Results and analysis

3.1 Establishment of mapping laws: Optimal QF-Q pairs and linear models

3.1.1 Identification of optimal QF-Q pairs

Figures 1 through 3 depict the calculated bpp correlation values for each image set (color, grayscale, and infrared) across all combinations of JPEG QF and BPG parameter Q. The analysis includes linear correlation (LCC) and rank-order correlations (KRCC and SRCC). In these figures, the maximum correlation value for each fixed value Q is highlighted with a black circle.

The results demonstrate that certain QF-Q combinations yield exceptionally high correlation values, confirming a strong predictable relationship between JPEG and BPG bpp for these specific parameter pairs. A clear inverse relationship between the parameters is observed: lower JPEG QF values (indicating lower image quality) correspond to higher BPG Q values (also indicating lower quality), and vice versa. Furthermore, the trends of these high-correlation QF-Q pairs exhibit notable similarity across all three image subsets, suggesting a fundamental and consistent relationship between the two compression methods.

Figure 4 summarizes the maximum correlation values achievable for each BPG Q parameter across all three image subsets and all three correlation methods. A key finding is that for the vast majority of Q values, the maximum attainable Pearson's (LCC) and Spearman's (SRCC) correlations exceed 0.98, indicating an exceptionally strong linear and monotonic relationship suitable for accurate prediction. The only exceptions are observed at very high compression ratios, where the parameter Q approaches its maximum value of 51; in this extreme regime, the correlation maxima are notably lower, suggesting a degradation in the predictability of the bpp relationship under severe compression. Furthermore, as theoretically expected, the Kendall correlation (KRCC) values are consistently lower than both Spearman's and Pearson's correlations across all Q values.

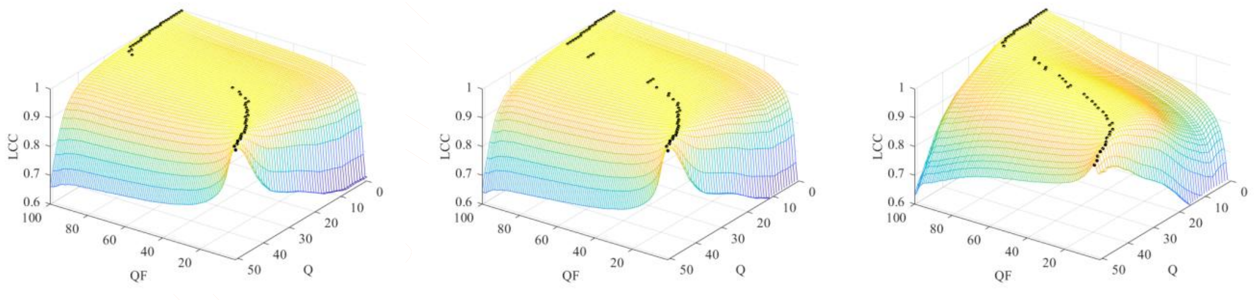

(a) color (b) grayscale (c) infrared

Fig. 1. Pearson correlation between JPEG and BPG bpp across image types

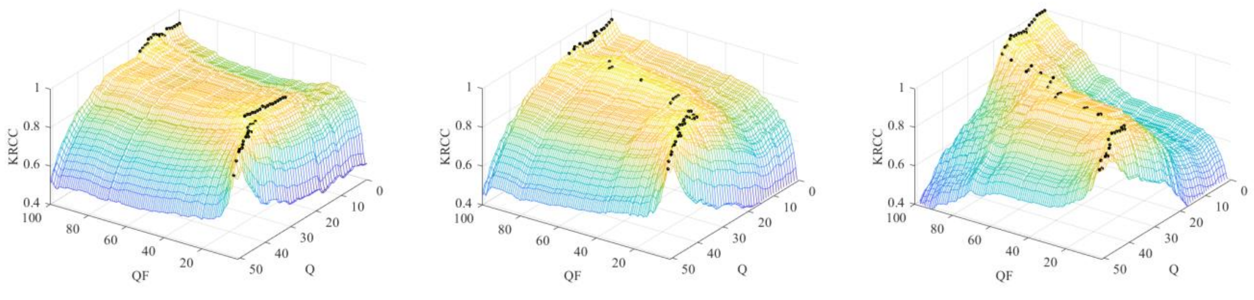

(a) color (b) grayscale (c) infrared

Fig. 2. Kendall correlation between JPEG and BPG bpp across image types

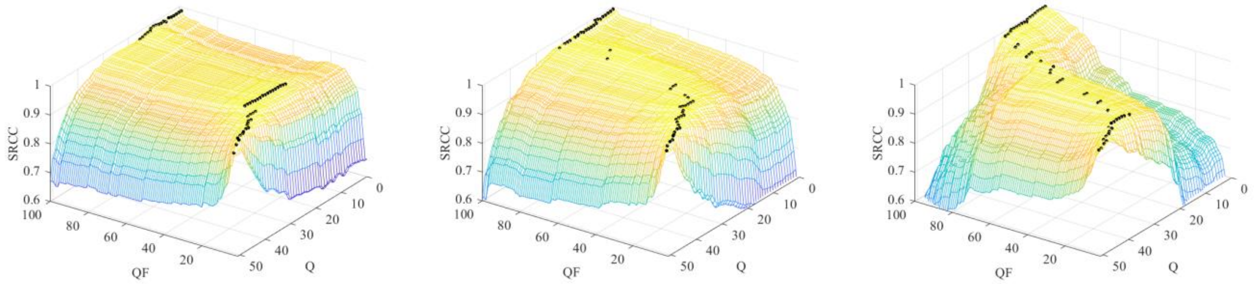

(a) color (b) grayscale (c) infrared

Fig. 3. Spearman correlation between JPEG and BPG bpp across image types

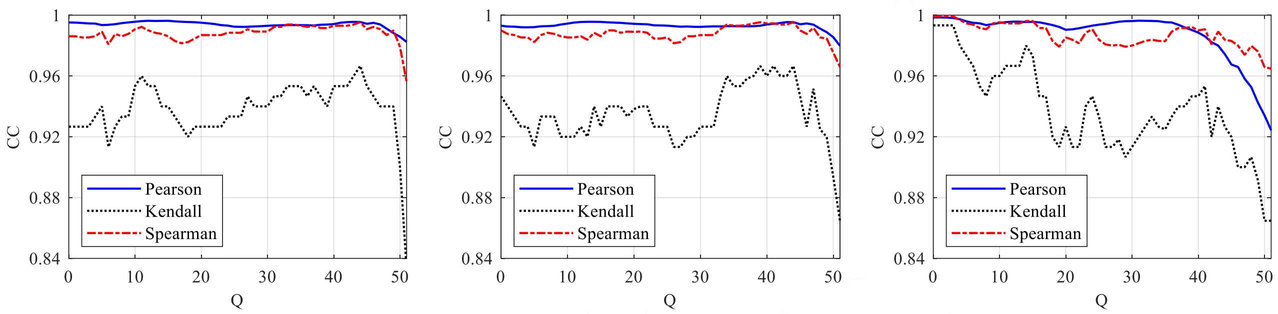

(a) color (b) grayscale (c) infrared

Fig. 4. Maximum values of correlations across image types

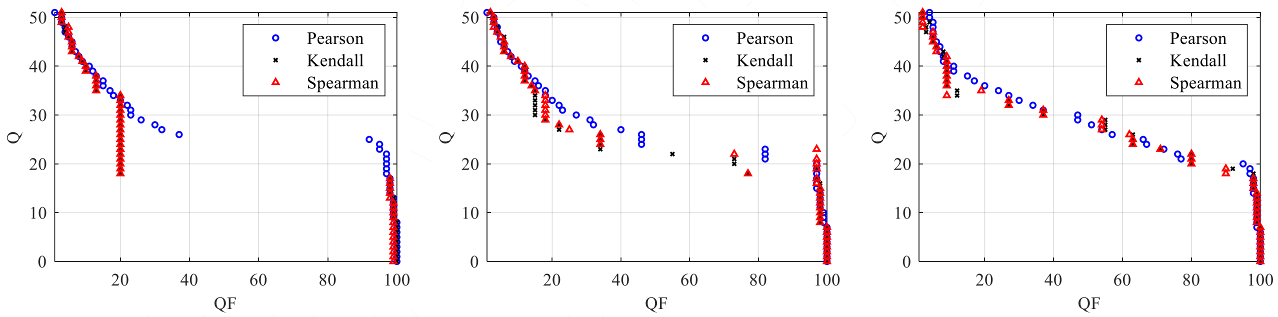

(a) color (b) grayscale (c) infrared

Fig. 5. JPEG QF vs BPG Q for maximum values of correlations across image types (all criteria)

Figure 5 presents the optimal combinations of JPEG QF and BPG Q parameters that yield these maximum bpp correlations, shown for all three image subsets and correlation methods. A notable observation is that the optimal parameter pairs for the rank-order correlations (KRCC and SRCC) are more consistent with each other than those for the linear correlation (LCC). Furthermore, Fig. 5 (see also Figs. 1-3) reveal discontinuities, or large jumps, in the sequence of optimal QF values as Q increases. These discontinuities can potentially affect the smoothness of predictions. While additional fine-tuning of the parameter pairs could mitigate these effects, some level of discontinuity is inherent due to the discrete nature of the QF (1-100) and Q (0-51) parameters, their differing dynamic ranges, and the fundamentally non-linear relationship between the two compression standards.

3.1.2 Illustration of linear mapping laws

Figures 6 through 8 illustrate the relationship between the bpp of JPEG and BPG-compressed images for the optimal combinations of parameters QF and Q, where optimality was defined by maximizing the linear Pearson correlation. To represent the bpp relationship across the entire quality spectrum, three target values of the BPG parameter Q were selected: 0 (highest quality), 26 (medium quality), and 51 (lowest quality). The corresponding optimal JPEG QF values used for each case are annotated below the figures.

A strong linear trend is evident in all three selected cases and across all image sets (color, grayscale, and infrared), visually confirming the high linear correlation values reported in Fig. 4. However, the spread of data points around the regression line varies significantly with the compression level. The spread is minimal for high-quality images (Q=0), indicating a very tight and predictable linear relationship. Conversely, the spread is most pronounced for low-quality images (Q=51), suggesting that the bpp relationship becomes noisier and slightly less deterministic under aggressive compression. This observed increase in variance aligns with the previously noted decrease in maximum correlation values for high Q parameters, as shown in Fig. 4.

Figure 6 illustrates the extreme case of maximum compression, where BPG uses its highest quantization parameter (Q=51) and prediction relies on correspondingly low JPEG quality factors (QF=1 for color and grayscale, QF=4 for infrared images). Without considering visual quality, the data reveals that BPG compression achieves a significantly higher compression ratio than JPEG, in some cases by more than an order of magnitude (a factor of 10). In contrast, Fig. 8 represents the opposite extreme case, with BPG at Q=0 and JPEG at QF=100. For this case, where compressed images are visually indistinguishable from the originals, the bpp (and consequently the CR), for JPEG and BPG are practically identical. This demonstrates that the superior compression efficiency of BPG manifests at lower quality levels, while both codecs converge to similar bitrates when targeting the highest fidelity.

3.1.3 Practical application of the mapping framework

The established mapping laws enable a practical framework for predicting BPG compression performance without executing the computationally intensive BPG encoding.

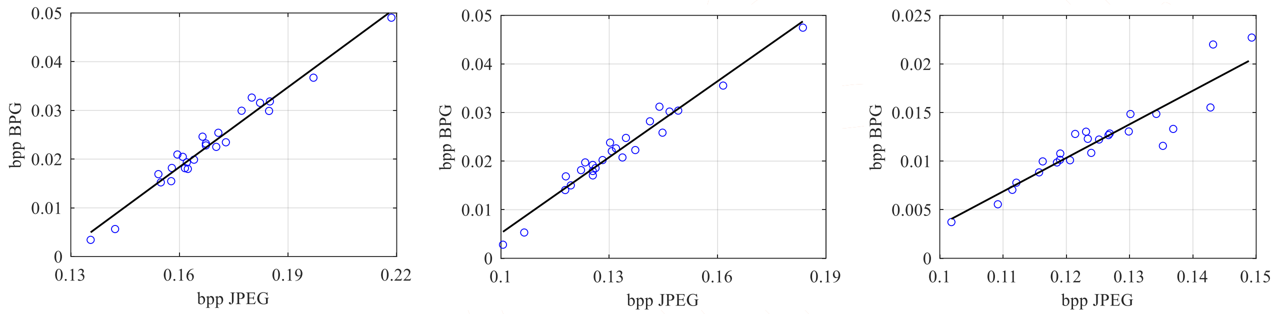

(a) color (QF=1) (b) grayscale (QF=1) (c) infrared (QF=4)

Fig. 6. Relationship between JPEG and BPG bpp for Q=51

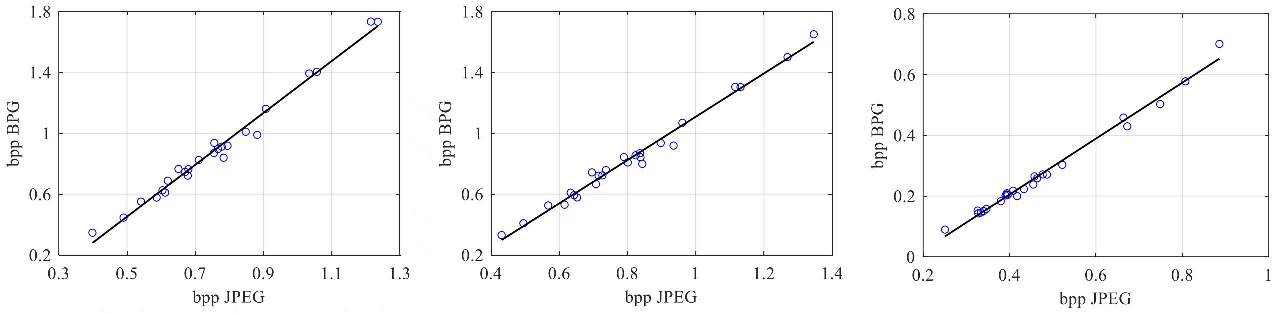

(a) color (QF=37) (b) grayscale (QF=46) (c) infrared (QF=57)

Fig. 7. Relationship between JPEG and BPG bpp for Q=26

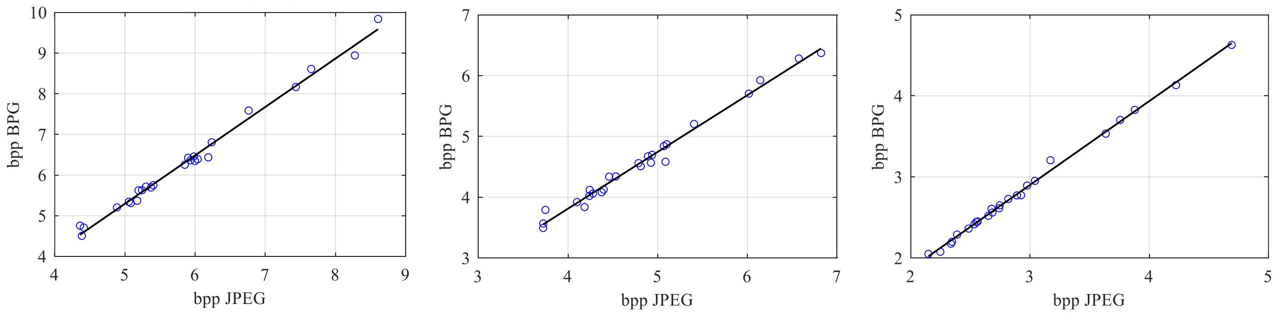

(a) color (QF=100) (b) grayscale (QF=100) (c) infrared (QF=100)

Fig. 8. Relationship between JPEG and BPG bpp for Q=0

To predict the bpp for a target BPG Q value, the corresponding optimal JPEG QF (as identified in Section 3.1.1 and Fig. 5) is first retrieved. The input image is then compressed using this specific JPEG QF setting – a relatively fast operation. The resulting JPEG bpp is used as input to the corresponding pre-derived linear mapping law (illustrated in Section 3.1.2 and Figs. 6-8) to obtain the predicted BPG bpp. This process effectively substitutes a single, fast JPEG compression for a slower BPG compression.

It is noteworthy that the framework is bidirectional in theory. Predicting JPEG bpp from a BPG compression would require an analogous set of 100 mapping laws (one for each QF from 1 to 100). However, the primary application value lies in predicting the performance of the more complex codec (BPG) using the simpler one (JPEG) as a proxy.

This approach is particularly advantageous in scenarios requiring rapid estimation of compression efficiency, such as bitrate allocation or algorithm selection, especially when using modern, complex codecs like BPG or VVC, whose encoding speeds can be far from real-time. The proposed method leverages the established linear relationships to bypass this computational bottleneck entirely.

3.2 Prediction performance on test scenarios

The core objective of this work is to predict the bpp of BPG compressed images without performing the actual BPG compression. This is achieved using the framework established in Section 3.1, which requires two key components: the optimal pairs of JPEG QF and BPG Q parameters (Fig. 5) and the corresponding linear mapping laws that translate JPEG bpp to BPG bpp. These 52 mapping laws are determined once in advance during the training phase. To validate this prediction framework, it was rigorously evaluated under two distinct testing scenarios to assess its accuracy and generalizability. Following the experimental setup described in Section 2.1, comprehensive tests were conducted where the bpp of a JPEG compressed image was used as input to the mapping laws to predict the BPG bpp. The evaluation leverages the correlation and error metrics defined in Section 2.4, including LCC, SRCC, KRCC, MAE, RMSE and MRE. The results are organized to first examine the model's intra-dataset performance on the M^3FD database, followed by a more challenging cross-dataset and cross-sensor evaluation.

3.2.1 Scenario 1: Intra-dataset performance

This section evaluates the prediction performance using the optimal mapping laws derived in Section 3.1. A comparative analysis is conducted between the predicted bpp values and the actual (observed) bpp values obtained from true BPG compression across the full range of the BPG quantization parameter Q (0 to 51).

The evaluation is performed on 25 image triplets from the M^3FD dataset, captured by the same sensor systems used in the training phase but explicitly excluded from the optimization process itself. This set includes images from both the visible and infrared parts of the electromagnetic spectrum. For each image and for every value of Q, the BPG bpp is predicted by applying the corresponding precomputed mapping law to the bpp of the JPEG compressed image (obtained using its optimal QF). These predictions are then compared against the true bpp values from the BPG compression to calculate the performance metrics.

Figure 9 illustrates the relationship between the predicted and true bpp values for color images. Since the analysis encompasses 25 source images across the full range of BPG Q values (0 to 51), both scatter plots in the figure comprises 1300 data points (25 images×52 parameter values).

Figure 9(a) presents the results segmented into five distinct subsets based on the Q parameter: 0-11, 12-21, 22-31, 32-41, and 42-51. This segmentation allows for a detailed analysis of prediction accuracy across different compression intensities. In contrast, Fig. 9(b) organizes the same data by source image, using different symbols and colors to represent the 25 groups of points, with each group containing 52 points corresponding to all Q values for a single original image. This visualization helps in assessing the consistency of the prediction model across different image contents.

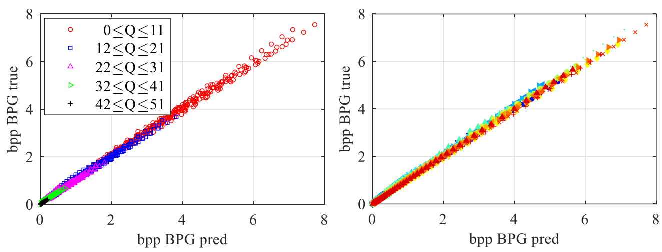

Fig. 9. Relationship between predicted and true bpp for color images: (a) distribution across Q sub-ranges, and (b) distribution across source images

Analysis of data in Fig. 9 confirms a high correlation between the predicted and true bpp values, validating the effectiveness of the mapping laws. The scatter plots stratified by Q sub-ranges, Fig. 9(a), reveal that the greatest dynamics in bpp values occur within the high-quality compression range (0≤Q≤11), where the parameter exerts the most substantial influence on bpp. Furthermore, the view grouped by source images, Fig. 9(b), demonstrates a consistent linear relationship between predictions and ground truth across all individual images, indicating the robustness of the method regardless of specific image content.

An identical analytical procedure was applied to assess the prediction performance for grayscale images. The evaluation was conducted on a set of 25 grayscale images, which were converted from the color images used in the previous analysis. The prediction process, following the same framework as for color images, yielded the results presented in Fig. 10.

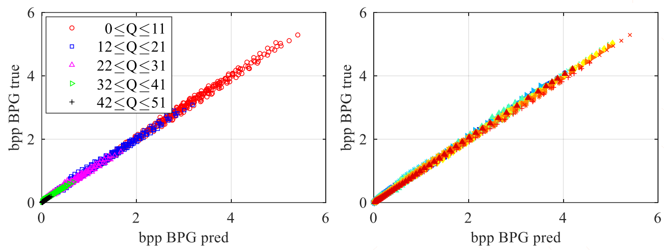

(a) (b)

Fig. 10. Relationship between predicted and true bpp for grayscale images: (a) distribution across Q sub-ranges, and (b) distribution across source images

The results for grayscale images, presented in Fig. 10, similarly demonstrate a high degree of correlation between the predicted and true bpp values. All key observations noted for color images remain valid: the data stratified by Q sub-ranges exhibits the same pattern of high bitrate dynamics at low Q values, while the data grouped by individual source images maintains a strong and consistent linear relationship. This consistency across image types underscores the robustness and general applicability of the proposed prediction framework within the same dataset.

The prediction results for BPG compressed infrared images are presented in Fig. 11.

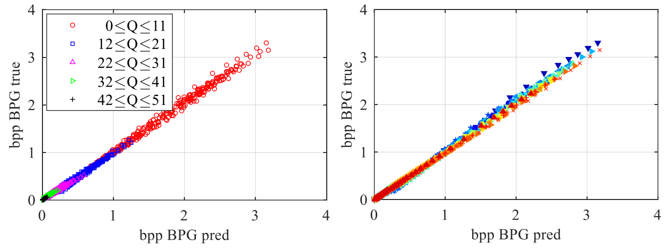

(a) (b)

Fig. 11. Relationship between predicted and true bpp for infrared images: (a) distribution across Q sub-ranges, and (b) distribution across source images

The evaluation was performed on a set of 25 original infrared images that are spatially aligned with the color and grayscale scenes previously analyzed, ensuring a direct comparison across spectral bands. The analysis of infrared images in Fig. 11 confirms that the high correlation between predicted and true bpp values is maintained, extending the validity of the proposed method to the infrared spectrum. The observations established for color and grayscale images, regarding the data distribution across Q sub-ranges and the linear relationship within individual source images, hold true in this case as well, demonstrating the robustness of the mapping framework across different image modalities.

A comparative analysis of the scatter plots in Figs. 9 to 11 reveals distinct dynamic ranges for the bpp values of each image type. Color images exhibit the widest range, with bpp values extending up to 8 (recall that original images are 24-bit). Grayscale images, as expected, show a more constrained range of up to 5.5 bpp, while infrared images display the narrowest dynamic range, reaching approximately 3.5 bpp. This progression aligns with the decreasing data volume inherent to each image modality. Notably, despite these differences in dynamic range, the spread of data points around the regression line (indicating prediction error) remains relatively consistent across all three types.

The quantitative assessment of the prediction agreement is summarized in Tab. 1, which presents the performance metrics for all three image types. The table provides a comprehensive overview through three correlation coefficients, alongside the MAE, RMSE, and MRE – calculated as the average of absolute differences between predicted and true values, divided by the true values. Together, these metrics offer relational, absolute error, and relative error perspectives on the model's accuracy.

Table 1. Quantitative evaluation of bpp prediction accuracy for color, grayscale, and infrared images

	color	grayscale	infrared
LCC	0.9991	0.9991	0.9990
SRCC	0.9986	0.9986	0.9990
KRCC	0.9701	0.9697	0.9748
MAE	0.0485	0.0379	0.0210
RMSE	0.0741	0.0541	0.0388
MRE (%)	8.4448	8.5098	6.2073

The results in Tab. 1 demonstrate an excellent agreement between the predicted and true bpp values. Both the LCC and SRCC correlation coefficients are consistently very high, approaching the ideal value of 1 across all image types. This strong performance is further supported by the KRCC values, which are also high, stable, and approximately 0.97.

Regarding prediction errors, the MAE and RMSE values are relatively low, confirming the model's practical accuracy. The lowest MAE and RMSE values are achieved for infrared images, while the highest are observed for color images. This performance is further validated by the MRE, which is lowest in the infrared domain at 6.21%, compared to approximately 8.5% for both color and grayscale modalities. This consistent pattern across all error metrics underscores the superior predictability of infrared images within the proposed framework.

Despite the consistently high correlation coefficients, a further reduction in prediction errors remains desirable. This is particularly significant in the low bpp regime (e.g., for values less than 0.5), where even small absolute errors can represent a substantial relative deviation. Enhancing prediction accuracy in this range is a crucial target for future refinements of the model.

This section analyzed bpp prediction for images from a publicly available database, employing a scenario where both training and testing phases utilize data from the same sensor system. This approach is not merely a methodological convenience but reflects a highly realistic use case. In practical applications, such as on a device with an embedded sensor capable of multiple compression types, the optimal strategy is to perform both model training (determining the mapping laws) and subsequent prediction using only images originating from that specific sensor. This self-contained framework would empower the device to select the optimal compression settings internally, requiring only a single, fast JPEG compression to predict the behavior of more complex codecs like BPG. Consequently, within this envisioned practical system, minimizing the prediction error becomes paramount for ensuring reliable and efficient performance.

The following section examines the universality of the proposed approach by evaluating bpp prediction for compressed images originating from other, external sensor systems.

3.2.2 Scenario 2: Cross-dataset and cross-sensor generalization

This section evaluates the universality and generalizability of the proposed prediction framework by testing it on images sourced from entirely different sensor systems and datasets. The optimal mapping laws, derived in the previous section from the M^3FD dataset, are now applied without any modification to predict the bpp of BPG compressed images originating from these external sources.

The results of the bpp prediction for externally sourced color and grayscale images are presented in Figs. 12 and 13. A comparative analysis with the intra-dataset results (Figs. 9 and 10) reveals two key observations. First, a slight deviation from the ideal linear trend is apparent, accompanied by a marginally wider spread of data points in the 2D space. Second, the dynamic range of the predicted bpp values is broader in this scenario; for color images, it extends to 12 compared to the previous 8, and for grayscale images, to 7 compared to 5.5. This indicates that the external dataset contains images with greater variability in complexity.

Despite these minor deviations, which are expected when applying a fixed model to entirely new sensor data, the overall prediction results remain highly acceptable. This demonstrates a notable degree of robustness and successful generalization of the mapping laws beyond the sensor system they were trained on.

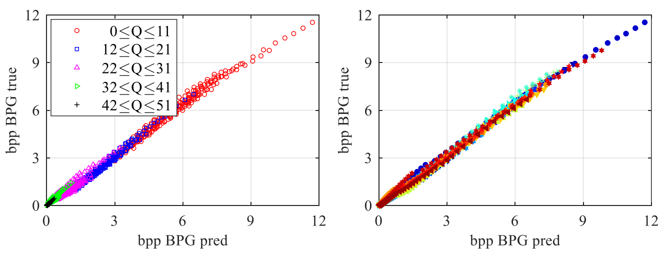

(a) (b)

Fig. 12. Relationship between predicted and true bpp for externally sourced color images: (a) distribution across Q sub-ranges, and (b) distribution across source images

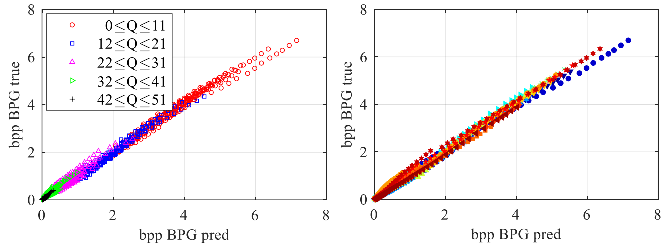

(a) (b)

Fig. 13. Relationship between predicted and true bpp for externally sourced grayscale images: (a) distribution across Q sub-ranges, and (b) distribution across source images

The prediction results for a set of 20 original infrared images from external sources are presented in Fig. 14. These infrared images do not correspond to the same scenes as the previously analyzed color and grayscale images. They were sourced from a publicly available infrared database and were captured using four distinct sensor systems, representing a significant diversification in data origin compared to the training set.

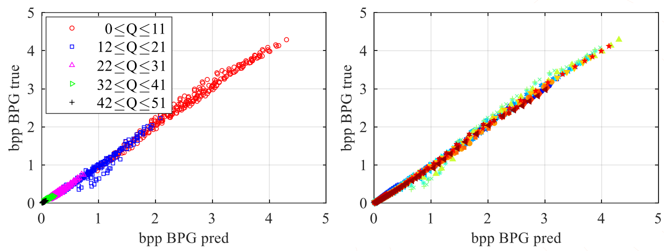

(a) (b)

Fig. 14. Relationship between predicted and true bpp for externally sourced infrared images: (a) distribution across Q sub-ranges, and (b) distribution across source images

Analysis of data in Fig. 14 reveals two critical findings. First, the dynamic range of bpp values for these external images is greater than that observed for the single sensor system used in the training phase (4.5 versus 3.5), indicating a wider variability in image complexity. Second, a slight but noticeable deviation from the linear trend is observed, particularly in the mid-range compression quality (12≤Q≤21). Crucially, the view grouped by source images, Fig. 14(b), reveals that this deviation is not uniformly distributed but is predominantly attributed to only four specific source images. Further analysis indicates that this deviation, while most pronounced in the mid-Q range (12-21), is also present for these same four images at lower Q values, albeit to a less noticeable degree.

Quantitative indicators of the prediction agreement for this external dataset are summarized in Tab. 2. A comparative analysis with the intra-dataset results (Tab. 1) confirms that, as expected, the performance is degraded when the model is applied to images from entirely different sensor systems.

Table 2. Quantitative evaluation of bpp prediction accuracy on external sensor data

	color	**grayscale**	**infrared**
LCC	0.9977	0.9973	0.9980
SRCC	0.9976	0.9972	0.9975
KRCC	0.9604	0.9562	0.9615
MAE	0.1414	0.0793	0.0434
RMSE	0.2288	0.1175	0.0769
MRE (%)	11.0391	9.7559	11.1261

Although the correlation values remain high, a marked increase in prediction errors is observed in this cross-sensor scenario. MAE is approximately three times higher for color images, two times higher for grayscale images, and two times higher for infrared images compared to the previous scenario. This pattern is further reflected in the MRE, with values of 11.04% for color, 9.76% for grayscale, and 11.13% for infrared compressed images. These relative errors are consistently higher than those observed in the intra-dataset evaluation, yet they remain within an acceptable range for practical applications, confirming the model's robustness when generalizing to unknown sensor data.

4 Conclusion

This paper presented and validated a novel methodology for predicting the bits per pixel (bpp) of BPG compressed images using only a fast JPEG pre-compression and precomputed linear mapping laws. The core finding is the existence of a strong, predictable relationship between the bpp of JPEG and BPG codecs, which holds with high accuracy both within a single sensor system and, with a moderate decrease in precision, across different and unknown sensors. This demonstrates that the computational burden of complex codecs like BPG can be effectively bypassed for rapid bitrate estimation in practical scenarios.

The proposed approach demonstrated high accuracy in the intra-dataset evaluation, with mean relative error (MRE) values of 6.21% for infrared, 8.51% for grayscale, and 8.44% for color images. More significantly, the framework maintained robust generalization to external sensor systems, where MRE values remained relatively low at 11.13% for infrared, 9.76% for grayscale, and 11.04% for color images. This consistent performance across different sensor systems confirms the practical utility of the proposed mapping methodology for bitrate prediction in diverse operational scenarios. For future work, this framework can be extended to other specialized domains like medicine or remote sensing. The core mapping principle can also be investigated for other codec pairs, with potential incorporation of non-linear models to further improve accuracy.

In conclusion, this paper has successfully established a method for predicting the bpp of BPG compression for any given quantization parameter Q and input image. A natural ensuing question is the practical application of this prediction. Currently, it enables a direct comparison of compression efficiency between JPEG and BPG. The logical next step is to integrate this with predictions of visual quality corresponding to the bpp values of these compressions. Existing intelligent quality prediction procedures, based on either PCC parameters or bpp itself, can be leveraged. Ultimately, by combining knowledge of both compression efficiency and perceived quality, an informed, automated decision can be made regarding the optimal compression type to use for a given image. This integration of bitrate and quality control will be a central focus of our future research.

References

[1] S. Jamil, "Review of Image Quality Assessment Methods for Compressed Images", *Journal of Imaging*, vol. 10, no. 5, art. no. 113, 2024, doi: 10.3390/jimaging10050113.

[2] A. Zemliachenko, R. Kozhemiakin, B. Vozel and V. Lukin, "Prediction of Compression Ratio in Lossy Compression of Noisy Images", *13th International Conference on Modern Problems of Radio Engineering, Telecommunications and Computer Science (TCSET)*, Lviv, Ukraine, 2016, pp. 693-697, doi: 10.1109/TCSET.2016.7452156.

[3] M.U.A. Ayoobkhan, E. Chikkannan and K. Ramakrishnan, "Lossy Image Compression Based on Prediction Error and Vector Quantisation", *EURASIP Journal on Image and Video Processing*, vol. 2017, no. 35, pp. 1-13, 2017, doi: 10.1186/s13640-017-0184-3.

[4] S. Pigeon and S. Coulombe, "Computationally Efficient Algorithms for Predicting the File Size of JPEG Images Subject to Changes of Quality Factor and Scaling", *24th Biennial Symposium on Communications*, Kingston, ON, Canada, 2008, pp. 378-382, doi: 10.1109/BSC.2008.4563280.

[5] S.-W. Wu and A. Gersho, "Rate-Constrained Picture-Adaptive Quantization for JPEG Baseline Coders", *IEEE International Conference on Acoustics, Speech, and Signal Processing*, Minneapolis, MN, USA, 1993, vol. 5, pp. 389-392, doi: 10.1109/ICASSP.1993.319829.

[6] A. Amirjanov and K. Dimililer, "Image Compression System with an Optimisation of Compression Ratio", *IET Image Processing*, vol. 13, no. 11, pp. 1960-1969, 2019, doi: 10.1049/iet-ipr.2019.0114.

[7] A. Zemliachenko, N. Ponomarenko, V. Lukin, K. Egiazarian and J. Astola, "Still Image/Video Frame Lossy Compression Providing a Desired Visual Quality", *Multidimensional Systems and Signal Processing*, vol. 27, no. 3, pp. 697-718, 2016, doi: 10.1007/s11045-015-0333-8.

[8] B. Bondžulić, B. Pavlović, N. Stojanović, V. Petrović and D. Bujaković, "A Simple and Reliable Approach to Providing a Visually Lossless Image Compression", *Visual Computer*, vol. 40, pp. 3747–3763, 2024, doi: 10.1007/s00371-023-03062-y.

[9] T. Chlubna and P. Zemčík, "Comparative Survey of Image Compression Methods Across Different Pixel Formats and Bit Depths", *Signal, Image and Video Processing*, vol. 19, no. 12, art. no. 981, 2025, doi: 10.1007/s11760-025-04579-6.

[10] M. Viitanen, J. Sainio, K. Siivonen, A. Mercat and J. Vanne, "uvg266: Open-Source VVC Intra Encoder", *32nd ACM International Conference on Multimedia*, Melbourne, Australia, 2024, pp. 11230-11233, doi: 10.1145/3664647.3685525.

[11] A. Yazdanpanah and M.R. Hashemi, "A New Compression Ratio Prediction Algorithm for Hardware Implementations of LZW Data Compression", *15th CSI International Symposium on Computer Architecture and Digital Systems*, Tehran, Iran, 2010, pp. 155-156, doi: 10.1109/CADS.2010.5623592.

[12] L. Li and Z.-S. Wang, "Compression Quality Prediction Model for JPEG2000", *IEEE Transactions on Image Processing*, vol. 19, no. 2, pp. 384-398, 2010, doi: 10.1109/TIP.2009.2034706.

[13] S. Pigeon and S. Coulombe, "K-Means Based Prediction of Transcoded JPEG File Size and Structural Similarity", *International Journal of Multimedia Data Engineering and Management*, vol. 3, no. 2, pp. 41-57, 2012, doi: 10.4018/jmdem.2012040103.

[14] R. Liu, Y. Zhang and Q. Zhou, "Research on Compression Performance Prediction of JPEG2000", *2nd International Symposium on Computer Engineering and Intelligent Communications (ISCEIC)*, Nanjing, China, 2021, pp. 278-284, doi: 10.1109/ISCEIC53685.2021.00065.

[15] B. Bondžulić, N. Stojanović, V. Petrović, B. Pavlović and Z. Miličević, "Efficient Prediction of the First Just Noticeable Difference Point for JPEG Compressed Images", *Acta Polytechnica Hungarica*, vol. 18, no. 8, pp. 201-220, 2021, doi: 10.12700/APH.18.8.2021.8.11.

[16] X. Tian, T. Li, J.-W. Tian and S. Li, "Prediction Method for Image Coding Quality Based on Differential Information Entropy", *Entropy*, vol. 16, no. 2, pp. 990-1001, 2014, doi: 10.3390/e16020990.

[17] V. Abramova, V. Lukin, S. Abramov, S. Kryvenko, P. Lech and K. Okarma, "A Fast and Accurate Prediction of Distortions in DCT-Based Lossy Image Compression", *Electronics*, vol 12, no. 11, art. no. 2347, 2023, doi: 10.3390/electronics12112347.

[18] А.Н. Осокин и Д.В. Сидоров, "Модифицированный кодер стандарта JPEG с контролем битрейта", *Интернет-журнал «НАУКОВЕДЕНИЕ»*, №5, 9 с., 2013, https://naukovedenie.ru/PDF/69tvn513.pdf.

[19] O. Murashko, J. Thomson and H. Leather, "Predicting and Optimizing Image Compression", *24th ACM International Conference on Multimedia*, Amsterdam, Netherlands, 2016, pp. 665-669, doi: 10.1145/2964284.2967305.

[20] V. Lukin, A. Zemliachenko, S. Abramov, B. Vozel and K. Chehdi, "Automatic Lossy Compression of Noisy Images by SPIHT or JPEG2000 in Optimal Operation Point Neighborhood", *6th European Workshop on Visual Information Processing (EUVIP)*, Marseille, France, 2016, pp. 1-6, doi: 10.1109/EUVIP.2016.7764581.

[21] H. Oh, A. Bilgin and M.W. Marcellin, "Visually Lossless Encoding for JPEG2000", *IEEE Transactions on Image Processing*, vol. 22, no. 1, pp. 189-201, 2013, doi: 10.1109/TIP.2012.2215616.

[22] V. Anisimovskiy, S. Zavalishin and I. Kurilin, "Fast JPEG Rate Control", *IS&T International Symposium on Electronic Imaging: Digital Photography and Mobile Imaging XII*, San Francisco, CA, USA, 2016, pp. DPMI-255.1-DPMI-255.9, doi: 10.2352/ISSN.2470-1173.2016.18.DPMI-255.

[23] Y. Liu, Z. Xiong, L. Lu and D. Hohl, "Fast SNR and Rate Control for JPEG XR", *10th International Conference on Signal Processing and Communication Systems (ICSPCS)*, Surfers Paradise, QLD, Australia, 2016, pp. 1-7, doi: 10.1109/ICSPCS.2016.7843328.

[24] N. Stojanović, B. Bondžulić, V. Lukin, D. Bujaković, S. Kryvenko and O. Ieremeiev, "Compression Ratio as Picture-Wise Just Noticeable Difference Predictor", *Mathematics*, vol. 13, no. 9, art. no. 1445, pp. 1-32, 2025, doi: 10.3390/math13091445.

[25] B. Bondžulić, N. Stojanović, V. Lukin and S. Kryvenko, "Visually Lossless Image Compression: From JPEG to BPG and Vice Versa", *IEEE Signal Processing Letters*, vol. 32, pp. 2942-2946, 2025, doi: 10.1109/LSP.2025.3587601.

[26] U. Albalawi, S.P. Mohanty and E. Kougianos, "A Hardware Architecture for Better Portable Graphics (BPG) Compression Encoder", *IEEE International Symposium on Nanoelectronic and Information Systems*, Indore, India, 2015, pp. 291-296, doi: 10.1109/iNIS.2015.12.

[27] Y. Zheng, G. Chen, Z. Wang and E. Blasch, "Image Quality (IQ) Guided Multispectral Image Compression", *Proc. of SPIE*, Baltimore, MD, USA, vol. 9871, art. no. 98710C, pp. 1-10, 2016, doi: 10.1117/12.2225532.

[28] J. Liu, X. Fan, Z. Huang, G. Wu, R. Liu, W. Zhong and Z. Luo, "Target-Aware Dual Adversarial Learning and a Multi-Scenario Multi-Modality Benchmark to Fuse Infrared and Visible for Object Detection", *IEEE/CVF Conference on Computer Vision and Pattern Recognition (CVPR)*, New Orleans, LA, USA, 2022, pp. 5802-5811, doi: 10.1109/CVPR52688.2022.00571.

[29] F. de Simone, L. Goldmann, V. Baroncini and T. Ebrahimi, "Subjective Evaluation of JPEG XR Image Compression", *Proc. of SPIE*, San Diego, CA, USA, vol. 7443, art. no. 74430L, pp. 1-12, 2009, doi: 10.1117/12.830714.

[30] L. Jin, J.Y. Lin, S. Hu, H. Wang, P. Wang, I. Katsavounidis, A. Aaron and C.-C. J. Kuo, "Statistical Study on Perceived JPEG Image Quality via MCL-JCI Dataset Construction and Analysis", *IS&T International Symposium on Electronic Imaging: Image Quality and System Performance XIII*, San Francisco, CA, USA, art. no. IQSP-222, pp. 1-9, 2016, doi: 10.2352/ISSN.2470-1173.2016.13.IQSP-222.

[31] O. Zelmati, B. Bondžulić, B. Pavlović, I. Tot and S. Merrouche, "Study of Subjective and Objective Quality Assessment of Infrared Compressed Images", *Journal of Electrical Engineering*, vol. 73, no. 2, pp. 73-87, 2022, doi: 10.2478/jee-2022-0011.

[32] F. Bellard, "BPG image format", Accessed: Nov. 11, 2025. [Online]. Available: https://bellard.org/bpg/

[33] Y. Wang and D. Mukherjee, "The Discrete Cosine Transform and Its Impact on Visual Compression: Fifty Years From Its Invention [Perspectives]", *IEEE Signal Processing Magazine*, vol. 40, no. 6, pp. 14-17, 2023, doi: 10.1109/MSP.2023.3282775.

Received 23 November 2025